

DOI: 10.1002/cctc.201402695

# Ni–Co/Al<sub>2</sub>O<sub>3</sub> Bimetallic Catalysts for CH<sub>4</sub> Steam Reforming: Elucidating the Role of Co for Improving Coke Resistance

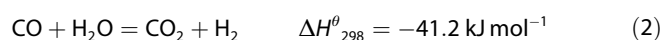
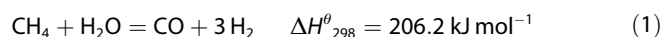
Xiaojuan You,<sup>[a]</sup> Xiang Wang,<sup>\*[a]</sup> Youhe Ma,<sup>[a]</sup> Jianjun Liu,<sup>[a]</sup> Wenming Liu,<sup>[a]</sup> Xianglan Xu,<sup>[a]</sup> Honggen Peng,<sup>\*[a]</sup> Changqing Li,<sup>[b]</sup> Wufeng Zhou,<sup>[b]</sup> Ping Yuan,<sup>[b]</sup> and Xiaohong Chen<sup>[b]</sup>

A series of supported Ni–Co/ $\gamma$ -Al<sub>2</sub>O<sub>3</sub> bimetallic catalysts with a fixed 12% Ni loading but different Co contents were prepared by using the coimpregnation method and investigated for methane steam reforming. The addition of Co can significantly improve the coke resistance and the reaction stability of Ni/Al<sub>2</sub>O<sub>3</sub> at a mild loss of the reforming activity. XPS and TEM results prove the existence of strong interaction between Ni and Co species. XRD and high-angle annular dark-field scan-

ning transmission electron microscopy mapping results of the reduced catalysts provide direct evidence for surface Ni–Co alloy formation upon Co addition onto Ni/Al<sub>2</sub>O<sub>3</sub>, which can block part of the active low coordinated Ni sites and lower the metal dispersion, thus effectively suppressing coking and improving the reaction stability in comparison with the unmodified Ni/Al<sub>2</sub>O<sub>3</sub> catalyst.

## Introduction

It is well-known that H<sub>2</sub> is a potential green-energy source with little pollution, and could be a long-term energy option for human being in the future. With the rapid development of industry and economy, the environment pollution becomes more and more severe, therefore, the demand for clean energy, such as hydrogen and solar energy, is growing very fast.<sup>[1,2]</sup> Hydrogen, as one of the important green-energy sources, might play a key role in the 21st century. Presently, methane steam reforming (MSR) is still the major and the most feasible route for large-scale industrial hydrogen production,<sup>[2]</sup> because of the abundant availability of natural gas and the relatively low cost compared with other methods. The main reactions involved in this process are described here.<sup>[3]</sup>



Owing to the strong endothermic property of reaction (1), a reformer generally operates at high temperatures (800–1100 °C)<sup>[4–6]</sup> and water is usually fed in excess to reduce coke formation and prolong the lifespan of the catalysts. For industrial-scale H<sub>2</sub> production, the commonly used steam-to-methane ratios are approximately 2.5–3.0.<sup>[7]</sup>

MSR is usually performed on the supported group VIII metals, such as Fe, Co, Ni, Pt, Pd, Ru, and Rh. Owing to its low price and high activity, Ni supported on different supports, such as  $\gamma$ -Al<sub>2</sub>O<sub>3</sub>,  $\alpha$ -Al<sub>2</sub>O<sub>3</sub>, MgO, CaAl<sub>2</sub>O<sub>4</sub>, or MgAl<sub>2</sub>O<sub>4</sub>, is most commonly used.<sup>[8–16]</sup> Although other group VIII metals are also reported to be active for the reaction, they have some drawbacks, for instance, iron is oxidized too rapidly to lose activity, cobalt is not able to withstand the high steam partial pressures, and the precious metals have generally limited source and too high costs. Therefore, to obtain a Ni-based catalyst with high activity and stability for large-scale H<sub>2</sub> production as an energy source, it is still necessary to design and develop catalysts with potent resistance to coking and active-site sintering, which are believed to be the two major reasons leading to the catalyst deactivation.<sup>[17–19]</sup> One of the commonly used solutions is the addition of basic metal oxides as promoters, such as MgO, CaO, and La<sub>2</sub>O<sub>3</sub>, CeO<sub>2</sub>.<sup>[20–23]</sup> Another method, the addition of a second active metal, has also been reported to be effective to improve the performance of the catalysts. For example, the bimetallic Ni–Co catalysts have been reported to show improved properties for some reactions, such as CO hydrogenation,<sup>[24–26]</sup> CH<sub>4</sub>/CO<sub>2</sub> reaction,<sup>[27–31]</sup> methane partial oxidation,<sup>[32]</sup> ethanol and acetic acid steam reforming.<sup>[33,34]</sup> Zhang et al.<sup>[30,31]</sup> investigated Ni/M/Al/Mg/O catalysts (M = Co, Fe, Cu, or Mn) and found that Ni–Co bimetallic catalysts have a superior performance for CO<sub>2</sub> reforming of CH<sub>4</sub> in terms of activity and stability to other Ni/M combination. In a 2000 h stability test, the Ni–Co catalyst displayed a very stable performance with very low carbon deposition. The excellent performance of the Ni–Co bimetallic catalyst could be closely related to its high metal dispersion, strong metal–support interaction, and formation of a stable solid solution. Chen et al.<sup>[27]</sup> investigated the effect of the Co–Ni ratio on the activity and stability of Co–Ni bimetallic aerogel catalysts for methane oxy–CO<sub>2</sub> reforming,

[a] X. You, Prof. Dr. X. Wang, Y. Ma, J. Liu, Dr. W. Liu, Dr. X. Xu, Dr. H. Peng  
College of Chemistry  
Nanchang University  
Nanchang, Jiangxi 330031 (P.R. China)  
Tel: (+86) 15979149877  
E-mail: xwang23@ncu.edu.cn  
penghonggen@ncu.edu.cn

[b] C. Li, W. Zhou, P. Yuan, X. Chen  
Jiangxi Golden Century Advanced Materials Co.Ltd.  
Nanchang, Jiangxi 330013 (P.R. China)

and found that the Co/Ni ratio has a strong influence on the catalytic performance, which was attributed to the formation of uniform metal alloy on the catalysts after reduction. In another study,<sup>[35]</sup> the authors also investigated the support and alloy effects on the activity and product selectivity for ethanol steam reforming over supported Ni–Co catalysts. The authors suggested that the support plays a very important role for the reaction. Yu et al.<sup>[36]</sup> revealed that a Ni–Co alloy was formed in the bimetallic catalysts. The interaction between Ni and Co improved the metal particle dispersion and resulted in smaller Ni size, thus increasing the catalytic activity and coke resistance. Studying CH<sub>4</sub> dry reforming on Co–Ni/TiO<sub>2</sub> catalysts, Aiwa et al. detected the formation of Ni–Co alloy on the catalyst surface, which significantly improves the coke resistance of the catalysts.<sup>[37]</sup> However, differently from the above-mentioned work by Zhang et al. and Yu et al., they found that the addition of Co decreased the dispersion of Ni active sites. Despite these conflict observations, it is commonly concluded that the addition of Co onto Ni-based catalysts can improve the reaction performance, especially for coke resistance. However, to the best of our knowledge, the application of supported bimetallic Ni–Co catalysts, especially Ni–Co/ $\gamma$ -Al<sub>2</sub>O<sub>3</sub>, for MSR has been rarely profiled.<sup>[38]</sup> Furthermore, the influence of the synergetic interaction between metallic Ni and Co on the reaction performance deserves further elucidation.

Aiming to solve these problems and to develop catalysts with potential industrial application, we prepared a series of supported Ni–Co/ $\gamma$ -Al<sub>2</sub>O<sub>3</sub> bimetallic catalysts with different Co contents but fixed Ni loading and investigated them for MSR. The results demonstrated that Co addition onto Ni/Al<sub>2</sub>O<sub>3</sub> catalysts leads to the formation of surface Ni–Co alloys, as evidenced by XRD analysis and high-angle annular dark-field scanning transmission electron microscopy (HAADF-STEM) mapping results, which effectively suppresses coke formation and improves the reaction stability in comparison with the unmodified Ni-based catalyst.

## Results

### Activity evaluation and stability test for Co–Ni/Al<sub>2</sub>O<sub>3</sub> catalysts with different Co contents

Our previous work has demonstrated that 12% Ni is the optimal loading for the  $\gamma$ -Al<sub>2</sub>O<sub>3</sub> used in this study.<sup>[39]</sup> As an endeavor to analyze the Co effects and develop better catalysts, this Ni loading was used for all the catalysts but the Co contents were varied. As shown in Figure 1, at temperatures below 800 °C, the unmodified catalyst exhibits the highest activity. The addition of 1% Co has little negative effect on the activity, but further increasing the Co contents degrades the activity evidently. The activity sequence is as follows: 12%Ni/Al<sub>2</sub>O<sub>3</sub>  $\approx$  1%Co–12%Ni/Al<sub>2</sub>O<sub>3</sub> > 7%Co–12%Ni/Al<sub>2</sub>O<sub>3</sub>  $\approx$  3%Co–12%Ni/Al<sub>2</sub>O<sub>3</sub> > 12%Co–12%Ni/Al<sub>2</sub>O<sub>3</sub>  $\approx$  15%Co–12%Ni/Al<sub>2</sub>O<sub>3</sub>. At 800 °C, the same methane conversion was achieved on all the catalysts.

To clarify the modification effects of Co on Ni/Al<sub>2</sub>O<sub>3</sub> catalysts, 7%Co–12%Ni/Al<sub>2</sub>O<sub>3</sub> was selected for further study, because

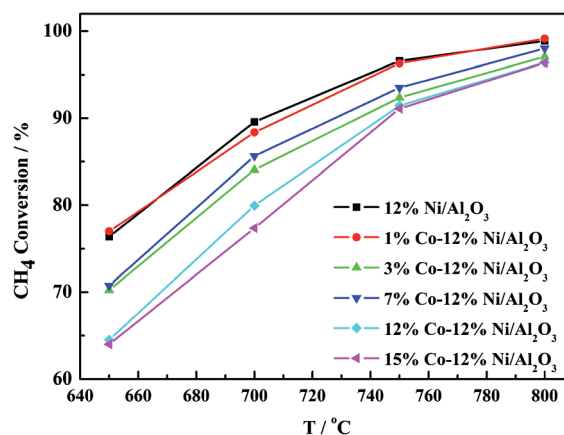


**Figure 1.** Reaction performance of the catalysts for MSR. Reaction conditions:  $p = 0.1$  MPa, GHSV = 18 000 mL g<sup>-1</sup> h<sup>-1</sup>, and H<sub>2</sub>O/CH<sub>4</sub> = 2:1.

coke formation on this sample could be suppressed thoroughly, which will be discussed in the following section. In addition, compared with that of the unmodified Ni/Al<sub>2</sub>O<sub>3</sub>, its activity decrease is not significant. Notably, though 1%Co–12%Ni/Al<sub>2</sub>O<sub>3</sub> has a high activity similar to that of the unmodified sample, stability tests indicate that methane conversion on it still drops gradually, implying the Co amount is not enough to suppress the carbon deposition completely, and slow deactivation still occurs.

The comparison of the reaction stability of 7%Co–12%Ni/Al<sub>2</sub>O<sub>3</sub> with that of 12%Ni/Al<sub>2</sub>O<sub>3</sub> and 12%Co/Al<sub>2</sub>O<sub>3</sub> is shown in Figure 2. Under the stringent condition adopted in this study, 12%Co/Al<sub>2</sub>O<sub>3</sub> exhibits low activity and very fast deactivation. In comparison, 12%Ni/Al<sub>2</sub>O<sub>3</sub> is much more active than 12%Co/Al<sub>2</sub>O<sub>3</sub> but its methane conversion decreases evidently from the initial 95% to 80% after 80 h, because of the presence of coke formation. However, 7%Co–12%Ni/Al<sub>2</sub>O<sub>3</sub> displays very stable reforming activity, as testified by the stable methane conversion remaining at 95% during the 180 h test. Obviously, although supported Ni or Co alone is not a good catalyst for the

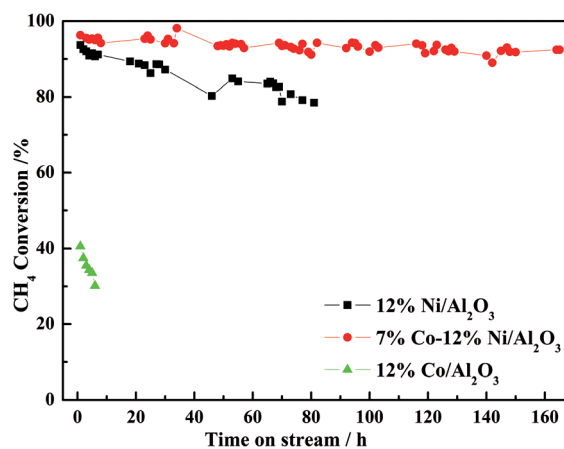


**Figure 2.** Comparison of the reaction stability of 7%Co–12%Ni/Al<sub>2</sub>O<sub>3</sub> with that of 12%Ni/Al<sub>2</sub>O<sub>3</sub> and 12%Co/Al<sub>2</sub>O<sub>3</sub> for MSR. Reaction conditions:  $p = 0.1$  MPa, GHSV = 18 000 mL g<sup>-1</sup> h<sup>-1</sup>, and H<sub>2</sub>O/CH<sub>4</sub> = 2:1,  $T = 800$  °C.

reaction, the combination of the two metals can result into Ni-Co bimetallic catalysts with superior performance.

### Thermogravimetric analysis differential scanning calorimetry and SEM investigation for the coke resistance of 7%Co–12%Ni/Al<sub>2</sub>O<sub>3</sub>

To elucidate the inherent reasons leading to the superior performance of the supported bimetallic Ni-Co catalysts, the coking amount of the spent catalysts after long-term stability tests was analyzed by thermogravimetric analysis differential scanning calorimetry (TGA–DSC) techniques (Figure 3). For 12%Ni/Al<sub>2</sub>O<sub>3</sub>, as shown in Figure 3(A), a significant weight loss

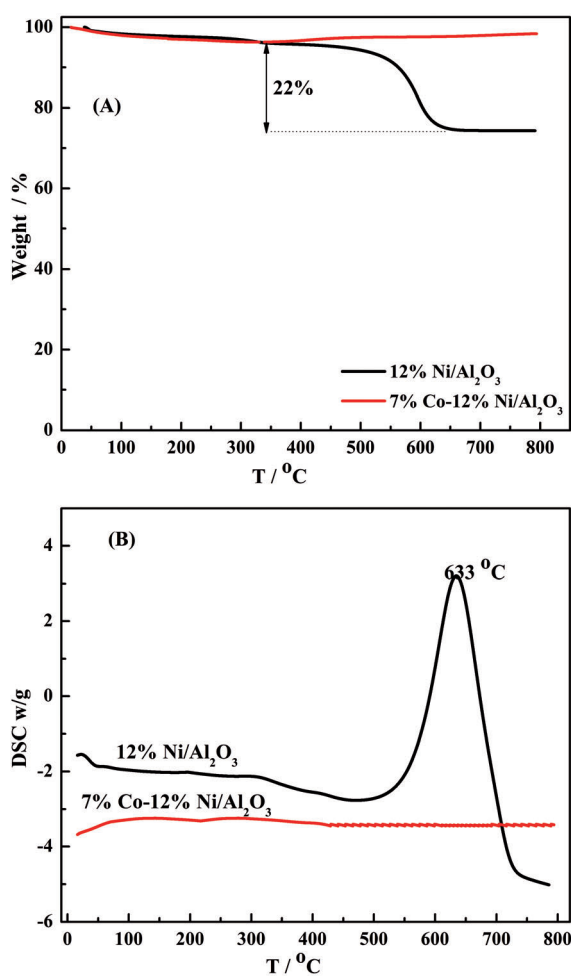


**Figure 3.** A) TGA and B) DSC profiles of catalysts after the long-term stability test.

stage with a weight loss of 22% is observed at 500–650 °C, which is accompanied by a strong exothermic peak ascribed to coke combustion at the same temperature region in Figure 3(B).<sup>[40]</sup> For 7%Co–12%Ni/Al<sub>2</sub>O<sub>3</sub>, interestingly, no clear weight loss stage on its TGA profile and no exothermic peak on its DSC curve can be observed in the same temperature region. Based on the first 80 h reaction results, 12%Ni/Al<sub>2</sub>O<sub>3</sub> has a coking rate of 2.7 mg<sub>cat.</sub><sup>-1</sup>h<sup>-1</sup>, and that for 7%Co–

12%Ni/Al<sub>2</sub>O<sub>3</sub> is 0 mg<sub>cat.</sub><sup>-1</sup>h<sup>-1</sup>, suggesting the addition of 7%Co suppresses the coke formation completely. Apparently, the addition of Co can improve the coking resistance of Ni/Al<sub>2</sub>O<sub>3</sub> without significant loss of its activity.

The SEM images of the fresh and used 7%Co–12%Ni/Al<sub>2</sub>O<sub>3</sub> and 12%Ni/Al<sub>2</sub>O<sub>3</sub> are shown in Figure 4. Compared with the clean surface of fresh 12%Ni/Al<sub>2</sub>O<sub>3</sub> shown in Figure 4(a), whisker-like carbon deposits are clearly present on the surface of the catalyst used for 80 h, as shown in Figure 4(b). The results

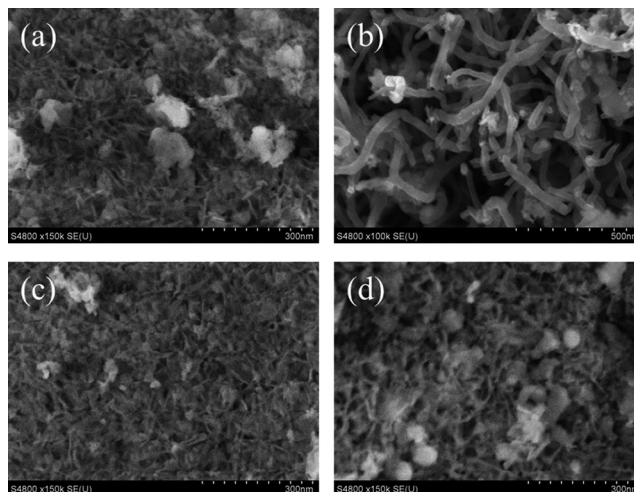


**Figure 4.** SEM images of the catalysts. a) Fresh 12%Ni/Al<sub>2</sub>O<sub>3</sub>, b) spent 12%Ni/Al<sub>2</sub>O<sub>3</sub>, c) fresh 7%Co–12%Ni/Al<sub>2</sub>O<sub>3</sub>, d) spent 7%Co–12%Ni/Al<sub>2</sub>O<sub>3</sub>. Scale bars: a) 300 nm, b) 500 nm, c) 300 nm, d) 300 nm.

are consistent with the previous findings on hydrocarbon dry reforming over Ni-based catalysts.<sup>[41–44]</sup> In contrast, for 7%Co–12%Ni/Al<sub>2</sub>O<sub>3</sub>, even after 180 h reaction time, no carbon deposit can be observed, as shown by the images of the fresh and the used catalysts in Figure 4(c) and (d), respectively. These SEM results agree very well with the coke formation rates obtained from TGA–DSC analysis and thus provide additional evidence that the addition of Co can effectively reduce and suppress coking on the supported Ni catalysts for CH<sub>4</sub> steam reforming.

### N<sub>2</sub>–BET, XRD, and H<sub>2</sub> temperature programmed reduction analysis of the fresh catalysts

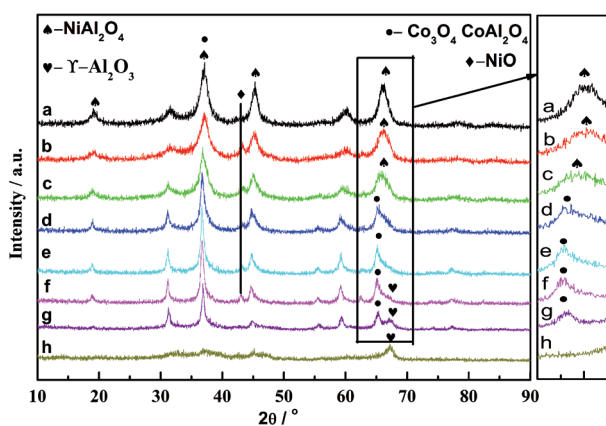
The specific surface areas of the fresh samples are listed in Table 1.  $\gamma$ -Al<sub>2</sub>O<sub>3</sub> support has a surface area of 137 m<sup>2</sup>g<sup>-1</sup>. The addition of 12% Ni or Co drops its surface area to approximately 110 m<sup>2</sup>g<sup>-1</sup>. The addition of Co and Ni together further decreases the surface areas of the prepared bimetallic catalysts. In addition, the more amount of Co is added, the lower the surface area becomes. It is therefore suggested that the decrease of the specific surface areas is one of the reasons for the decreased reforming activity of the Co-modified samples at low temperatures.

XRD and H<sub>2</sub> temperature programmed reduction (H<sub>2</sub>–TPR) analyses were used together to identify the phase compositions of the fresh catalysts, with the XRD patterns shown in

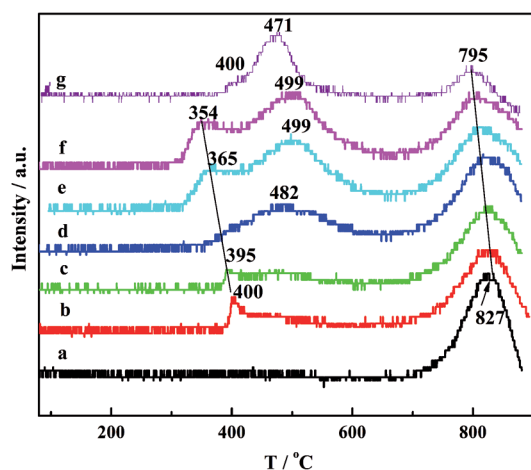
Sample	Surface area [m <sup>2</sup> g <sup>-1</sup> ]	Phase composition analyzed by XRD and H <sub>2</sub> -TPR
12%Ni/Al <sub>2</sub> O <sub>3</sub>	109	NiAl <sub>2</sub> O <sub>4</sub>
1%Co-12%Ni/Al <sub>2</sub> O <sub>3</sub>	106	NiAl <sub>2</sub> O <sub>4</sub> , NiO, Co <sub>3</sub> O <sub>4</sub> , CoAl <sub>2</sub> O <sub>4</sub>
3%Co-12%Ni/Al <sub>2</sub> O <sub>3</sub>	99	NiAl <sub>2</sub> O <sub>4</sub> , NiO, Co <sub>3</sub> O <sub>4</sub> , CoAl <sub>2</sub> O <sub>4</sub>
7%Co-12%Ni/Al <sub>2</sub> O <sub>3</sub>	94	NiAl <sub>2</sub> O <sub>4</sub> , NiO, Co <sub>3</sub> O <sub>4</sub> , CoAl <sub>2</sub> O <sub>4</sub>
12%Co-12%Ni/Al <sub>2</sub> O <sub>3</sub>	81	NiAl <sub>2</sub> O <sub>4</sub> , NiO, Co <sub>3</sub> O <sub>4</sub> , CoAl <sub>2</sub> O <sub>4</sub>
15%Co-12%Ni/Al <sub>2</sub> O <sub>3</sub>	78	NiAl <sub>2</sub> O <sub>4</sub> , NiO, Co <sub>3</sub> O <sub>4</sub> , CoAl <sub>2</sub> O <sub>4</sub>
12%Co/Al <sub>2</sub> O <sub>3</sub>	113	Co <sub>3</sub> O <sub>4</sub> , CoAl <sub>2</sub> O <sub>4</sub>
γ-Al <sub>2</sub> O <sub>3</sub> support	137	γ-Al <sub>2</sub> O <sub>3</sub>

Figure 5 and H<sub>2</sub>-TPR profiles in Figure 6. The phase compositions of the catalysts are also listed in Table 1.

For the unmodified 12%Ni/Al<sub>2</sub>O<sub>3</sub>, all the diffraction peaks can be assigned to spinel NiAl<sub>2</sub>O<sub>4</sub> (Figure 5). In addition, the



**Figure 5.** XRD patterns of the fresh catalysts. a) 12%Ni/Al<sub>2</sub>O<sub>3</sub>, b) 1%Co-12%Ni/Al<sub>2</sub>O<sub>3</sub>, c) 3%Co-12%Ni/Al<sub>2</sub>O<sub>3</sub>, d) 7%Co-12%Ni/Al<sub>2</sub>O<sub>3</sub>, e) 12%Co-12%Ni/Al<sub>2</sub>O<sub>3</sub>, f) 15%Co-12%Ni/Al<sub>2</sub>O<sub>3</sub>, g) 12%Co/Al<sub>2</sub>O<sub>3</sub>, h) γ-Al<sub>2</sub>O<sub>3</sub>. Peaks characteristic for the respective phase compositions are indicated. The box shows an enlargement of the peak around 65.84°.



**Figure 6.** H<sub>2</sub>-TPR results of fresh catalysts with different Co contents. a) 12%Ni/Al<sub>2</sub>O<sub>3</sub>, b) 1%Co-12%Ni/Al<sub>2</sub>O<sub>3</sub>, c) 3%Co-12%Ni/Al<sub>2</sub>O<sub>3</sub>, d) 7%Co-12%Ni/Al<sub>2</sub>O<sub>3</sub>, e) 12%Co-12%Ni/Al<sub>2</sub>O<sub>3</sub>, f) 15%Co-12%Ni/Al<sub>2</sub>O<sub>3</sub>, g) 12%Co/Al<sub>2</sub>O<sub>3</sub>. The straight lines illustrate the shift in the peak maxima.

H<sub>2</sub>-TPR profile in Figure 6 of this sample reveals only a single reduction peak at 827 °C, which is attributed to the reduction of spinel NiAl<sub>2</sub>O<sub>4</sub>.<sup>[45]</sup> Clearly, NiO reacted thoroughly with the γ-Al<sub>2</sub>O<sub>3</sub> support during the high-temperature calcination, therefore, no free NiO was present in this sample. For 12%Co/Al<sub>2</sub>O<sub>3</sub>, the H<sub>2</sub>-TPR profile reveals two groups of reduction peaks. The first group of peaks at 400 and 471 °C are assigned to the step-wise reduction of Co<sub>3</sub>O<sub>4</sub>,<sup>[46,47]</sup> as testified by our quantification results, for which the H<sub>2</sub> consumption amount of the 471 °C to 400 °C peak is at the stoichiometric ratio of 3:1. The second group peak at 795 °C is assigned to the reduction of spinel CoAl<sub>2</sub>O<sub>4</sub>.<sup>[35]</sup> As both Co<sub>3</sub>O<sub>4</sub> and CoAl<sub>2</sub>O<sub>4</sub> have spinel structure and nearly the same XRD diffraction features, all the peaks of 12%Co/Al<sub>2</sub>O<sub>3</sub> can be assigned to the overlapping diffraction from both, except for the small peak at 67.14°, which is the strongest diffraction peak of the γ-Al<sub>2</sub>O<sub>3</sub> support. Apparently, Co<sub>3</sub>O<sub>4</sub> and CoAl<sub>2</sub>O<sub>4</sub> coexist in this sample but the amount of Co<sub>3</sub>O<sub>4</sub> is relatively larger, as evidenced by H<sub>2</sub>-TPR results.

For all of the Ni-Co bimetallic catalysts, with the increasing of Co amount, a diffraction peak at 19.14°, which can be safely assigned to spinel NiAl<sub>2</sub>O<sub>4</sub>, becomes smaller. Concurrently, a diffraction peak at 43.04°, which is assigned to NiO, appears in 1%Co-12%Ni/Al<sub>2</sub>O<sub>3</sub> and eventually becomes larger with the increasing amount of Co. This indicates that the addition of Co can impede the formation of spinel NiAl<sub>2</sub>O<sub>4</sub> effectively, thus keeping part of NiO free. Notably, a diffraction peaks at 31.60° becomes stronger with the addition amount of Co, which is obviously related to Co species. Moreover, all spinel NiAl<sub>2</sub>O<sub>4</sub>, Co<sub>3</sub>O<sub>4</sub>, and CoAl<sub>2</sub>O<sub>4</sub> exhibit diffraction peaks at approximately 37.02, 45.30, 60.00, and 65.84°, therefore, for these peaks of the catalysts, though they change slightly with the addition of Co, it is difficult to draw any definite conclusion based on them. However, it is still evident that with the addition amount of Co, the intensity of these peaks becomes weaker. Therefore, they could reflect the decrease of the amount of NiAl<sub>2</sub>O<sub>4</sub> in the catalysts. For clarification, the peak at 65.84° is enlarged and shown beside the major figure. Clearly, besides the intensity change, the peak also shifts to a smaller angle, and eventually close to that of the peak of 12%Co/Al<sub>2</sub>O<sub>3</sub>.

The H<sub>2</sub>-TPR results in Figure 6 also demonstrate that with the increasing Co amount, the reduction peak of spinel NiAl<sub>2</sub>O<sub>4</sub> becomes smaller, and that of NiO (350–400 °C) becomes larger, but both shift to lower temperature region. In comparison, the reduction peak at approximately 470–500 °C, which is assigned to the reduction of Co<sub>3</sub>O<sub>4</sub> in different chemical environment, becomes larger. As 12%Co/Al<sub>2</sub>O<sub>3</sub> displays a reduction peak of CoAl<sub>2</sub>O<sub>4</sub> at 795 °C, it is more reasonable to assign the high-temperature peak of all the bimetallic Ni-Co catalysts to the overlapping reduction of both NiAl<sub>2</sub>O<sub>4</sub> and CoAl<sub>2</sub>O<sub>4</sub>.

In summary, H<sub>2</sub>-TPR provides extra evidence to prove that the addition of Co can impede the formation of NiAl<sub>2</sub>O<sub>4</sub>, thus keeping part of NiO free on the catalyst surface, which may facilitate the formation of Ni-Co alloy during the reduction process. The formed alloy is believed to be important to increase the coke resistance of the Co-modified catalysts.<sup>[27,30]</sup> However, it was previously reported that the presence of Ni in the crystal matrix of NiAl<sub>2</sub>O<sub>4</sub> can hinder the growth of Ni particle size

during the pre-reduction for Ni catalysts prior to reaction, thus achieving catalysts with high activity.<sup>[46]</sup> The decrease of the amount of  $\text{NiAl}_2\text{O}_4$  in Ni–Co bimetallic catalysts could be negative for the activity, and might be one of the reasons accounting for their lowered reforming activity at low temperatures.

### X-ray photoelectron spectroscopy analysis of the fresh catalyst

X-ray photoelectron spectroscopy (XPS) analysis on the fresh catalysts was performed to obtain more insight into the surface properties of the bimetallic Ni–Co catalysts, with the results shown in Figure 7. For 12%Ni/ $\text{Al}_2\text{O}_3$  catalyst, the binding

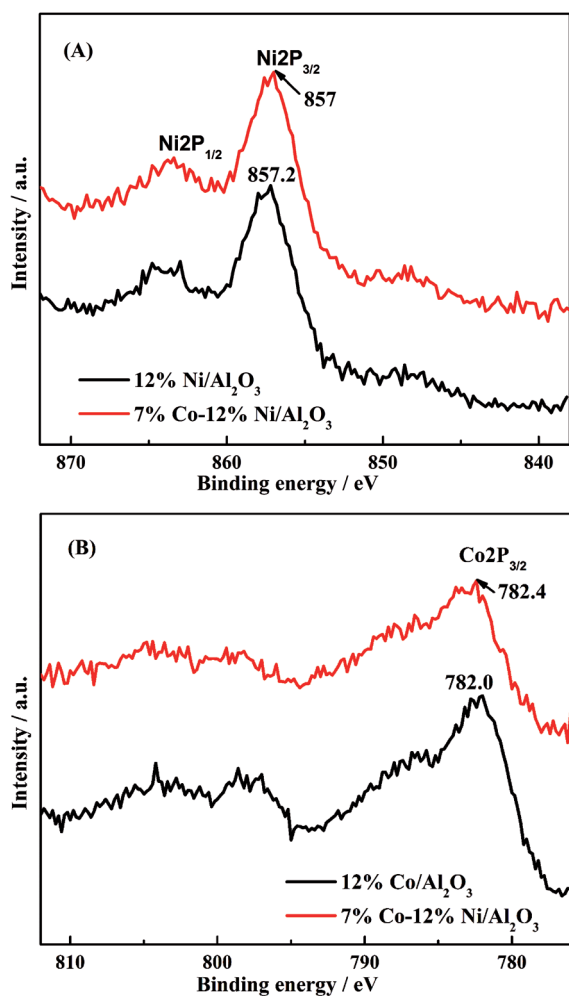


**Figure 7.** Comparison of A) Ni  $2p_{3/2}$  and B) Co  $2p_{3/2}$  XPS binding energies of the fresh 7%Co–12%Ni/ $\text{Al}_2\text{O}_3$  with those of 12%Ni/ $\text{Al}_2\text{O}_3$  and 12%Co/ $\text{Al}_2\text{O}_3$  catalysts, respectively.

energy of the Ni  $2p_{3/2}$  is 857.2 eV, which is assigned to the  $\text{Ni}^{2+}$  cations in  $\text{NiAl}_2\text{O}_4$ .<sup>[45]</sup> After Co addition, this peak shifts to 857.0 eV in 7%Co–12%Ni/ $\gamma\text{-Al}_2\text{O}_3$ , which could be affected by the presence of NiO and Co species. For 12%Co/ $\text{Al}_2\text{O}_3$  catalyst, the binding energy of the Co  $2p_{3/2}$  is 782.0 eV, which is ascribed to the  $\text{Co}^{2+}$  cations in both spinel  $\text{Co}_3\text{O}_4$  and  $\text{CoAl}_2\text{O}_4$ .<sup>[7,49,50]</sup>

However, the peak shifts to 782.4 eV in 7%Co–12%Ni/ $\gamma\text{-Al}_2\text{O}_3$ . Compared with the two monometallic Ni and Co samples, the combination of Ni and Co in the bimetallic 7%Co–12%Ni/ $\gamma\text{-Al}_2\text{O}_3$  obviously migrates the Ni  $2p_{3/2}$  peak to lower binding energy, but the Co  $2p_{3/2}$  peak to higher binding energy, suggesting that electron migration occurs between Ni and Co. This further confirms the close interaction between the two metals in the bimetallic catalysts, which may facilitate the Ni–Co alloy formation on the catalyst surface during reduction.<sup>[31,37]</sup>

### XRD and TEM studies on the reduced Co–Ni/ $\text{Al}_2\text{O}_3$ catalysts

XRD patterns of the reduced catalysts with different Co contents are shown in Figure 8. As all the catalysts were reduced at 800 °C, metallic Ni and Co are completely formed. The reduced 12%Ni/ $\text{Al}_2\text{O}_3$  and 12%Co/ $\text{Al}_2\text{O}_3$  display basically the same XRD diffraction patterns, indicating the diffraction of metallic Ni and Co are overlapped. Therefore, it is impossible

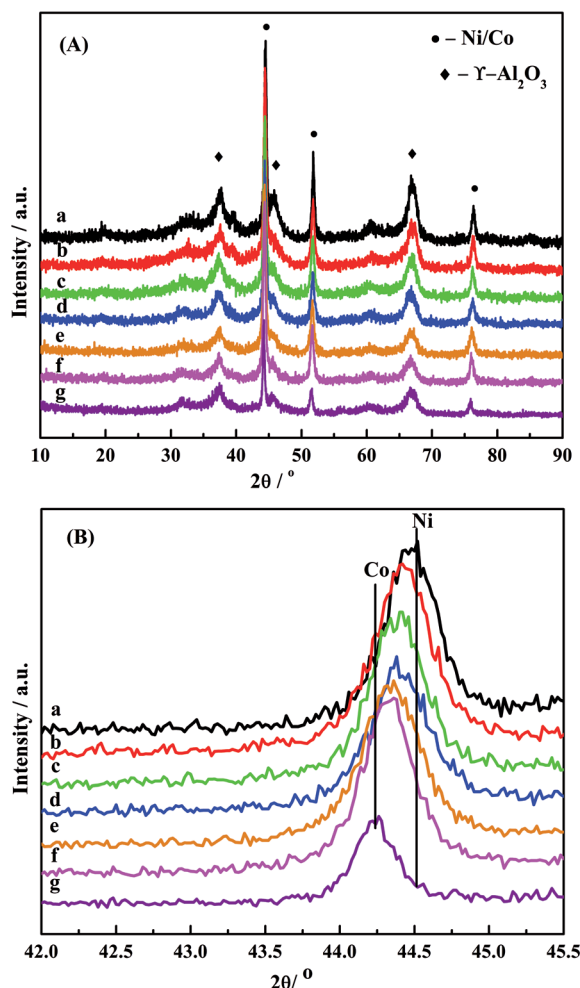


**Figure 8.** XRD patterns of the reduced catalysts. a) 12%Ni/ $\text{Al}_2\text{O}_3$ , b) 1%Co–12%Ni/ $\text{Al}_2\text{O}_3$ , c) 3%Co–12%Ni/ $\text{Al}_2\text{O}_3$ , d) 7%Co–12%Ni/ $\text{Al}_2\text{O}_3$ , e) 12%Co–12%Ni/ $\text{Al}_2\text{O}_3$ , f) 15%Co–12%Ni/ $\text{Al}_2\text{O}_3$ , g) 12%Co/ $\text{Al}_2\text{O}_3$ . A)  $2\theta$  range 10–90°; B)  $2\theta$  range 42.0–45.5°. Peaks characteristic for the respective phase compositions are indicated.

Sample	Ni crystallite size [nm] <sup>[a]</sup>	Ni particle size [nm] <sup>[b]</sup>	Ni/Co, <i>hkl</i> (111) $2\theta$ [°]	Ni/Co, <i>hkl</i> (111) <i>d</i> [Å]	Ni/Co, <i>hkl</i> (200) $2\theta$ [°]	Ni/Co, <i>hkl</i> (200) <i>d</i> [Å]
12%Ni/Al <sub>2</sub> O <sub>3</sub>	25.5	25.4	44.44	2.0371	51.80	1.7610
1%Co–12%Ni/Al <sub>2</sub> O <sub>3</sub>	29.6	30.3	44.42	2.0378	51.72	1.7635
3%Co–12%Ni/Al <sub>2</sub> O <sub>3</sub>	31.1	31.4	44.40	2.0386	51.70	1.7660
7%Co–12%Ni/Al <sub>2</sub> O <sub>3</sub>	28.1	27.0	44.38	2.0395	51.68	1.7673
12%Co–12%Ni/Al <sub>2</sub> O <sub>3</sub>	29.4	29.9	44.36	2.0400	51.66	1.7679
15%Co–12%Ni/Al <sub>2</sub> O <sub>3</sub>	31.8	31.4	44.34	2.0413	51.60	1.7698
12%Co/Al <sub>2</sub> O <sub>3</sub>	31.7	–	44.27	2.0457	51.56	1.7710

[a] Crystallite size calculated from XRD diffraction peak *hkl* (111). [b] Particle size measured by TEM.

to distinguish metallic Ni and Co from each other for those bimetallic samples. The crystallite sizes of the Ni/Co metals estimated using Scherrer's equation are listed in Table 2. The crystallite size of pure Ni<sup>0</sup> for the unmodified 12%Ni/Al<sub>2</sub>O<sub>3</sub> is 25.5 nm, and that of pure Co<sup>0</sup> for 12%Co/Al<sub>2</sub>O<sub>3</sub> is 31.7 nm. For all of the bimetallic samples, the crystallite sizes of the Ni/Co metals ranges from 28.1 to 31.8 nm, which are larger than that of pure Ni<sup>0</sup> and close to that of pure Co<sup>0</sup>. It was reported previously that the formation of alloy generally resulted in the growth of metal crystallite size.<sup>[37]</sup>

To further clarify this, the strongest diffraction peak, the (111) peak between 44 and 45° of each sample was enlarged and plotted separately in Figure 8(B). The  $2\theta$  peak of pure Ni<sup>0</sup> is at 44.44°, whereas that of pure Co<sup>0</sup> is at 44.27° (Table 2). Although the difference is very marginal, it is still possible to differentiate the peaks of the monometallic catalysts. However, for all bimetallic catalysts, only a uniform diffraction peak can be observed for the coexisted Ni<sup>0</sup> and Co<sup>0</sup> in the sample, which shifts to lower  $2\theta$  value gradually with the increasing of Co content, similar to what was reported on Ni<sub>m</sub>Co<sub>n</sub>/cordierite catalysts.<sup>[51]</sup> Additionally, the  $2\theta$  values of (200) peaks of the samples were also carefully measured and listed in Table 2, and a similar shift was observed. This peak shift is typical for alloy formation, suggesting that Ni–Co alloy is formed in the bimetallic catalysts during the reduction.<sup>[37]</sup>

The metal-particle morphology and size distribution of the reduced catalysts were investigated by TEM technique, with the images shown in Figure 9. The mean particle size of metallic Ni/Co measured by TEM for each sample is also listed in Table 2. For 12%Ni/Al<sub>2</sub>O<sub>3</sub> catalyst, the mean Ni<sup>0</sup> particle size is approximately 25.4 nm (Figure 9a). Notably, regular TEM technique and image cannot distinguish Ni<sup>0</sup> and Co<sup>0</sup>, therefore, the particles measured on the bimetallic sample surface actually consist of both metallic Ni and Co, which are Ni–Co alloy particles formed on the surface, as testified by XRD results. In line with the XRD results, the Ni–Co alloy particle sizes measured by TEM are larger than that of pure Ni<sup>0</sup> but close to that of Co<sup>0</sup>. In addition, all of the catalysts have similar crystallite and particle sizes, indicating the absence of the secondary aggregation of the Ni–Co alloy microcrystals. Regarding the Ni/Co distribution on the particle surface, the monometallic Ni sample exhibits monomodal distribution, indicating the only presence of one group of large particles. In comparison, all the bimetallic samples display bimodal distribution, revealing the

presence of two groups of large particles. Thus the results confirm that the added Co has strong interaction with Ni, which affects the chemical environment of both elements.

### H<sub>2</sub> adsorption–desorption measurements of the reduced Co–Ni/Al<sub>2</sub>O<sub>3</sub> catalysts

In Table 3, the metal dispersion results on the reduced samples measured by H<sub>2</sub> adsorption–desorption are listed. As all the samples were calcined and reduced at 800 °C, it is not surprising to find that they have generally low metal dispersion. 12%Ni/Al<sub>2</sub>O<sub>3</sub> catalyst has the highest metal dispersion, and

Catalyst	Metal dispersion [%]
12%Ni/Al <sub>2</sub> O <sub>3</sub>	9.2
1%Co–12%Ni/Al <sub>2</sub> O <sub>3</sub>	3.6
3%Co–12%Ni/Al <sub>2</sub> O <sub>3</sub>	2.1
7%Co–12%Ni/Al <sub>2</sub> O <sub>3</sub>	1.5
12%Co–12%Ni/Al <sub>2</sub> O <sub>3</sub>	0.8
15%Co–12%Ni/Al <sub>2</sub> O <sub>3</sub>	0.6
12%Co/Al <sub>2</sub> O <sub>3</sub>	0.8

12%Co/Al<sub>2</sub>O<sub>3</sub> catalyst has the lowest one among all of the samples. Although the intrinsic property of a metal could be the major reason to affect its activity, the metal dispersion can also influence its activity. Therefore, it is easy to understand that 12%Ni/Al<sub>2</sub>O<sub>3</sub> exhibit very high initial steam reforming activity, but the activity of 12%Co/Al<sub>2</sub>O<sub>3</sub> is extremely low, as shown in Figure 2. The addition of Co onto the samples apparently decreases the Ni/Co alloy dispersion. In addition, with the increasing of Co amount, the alloy dispersion keeps on decreasing. With the increasing of the Co content to 15%, the alloy dispersion on the sample is even slightly lower than that of pure 12%Co/Al<sub>2</sub>O<sub>3</sub>. It is commonly accepted that the oxidation activity of a supported metal catalysts is remarkably affected by the exposed metal surface. Regularly, on the same support, the higher the metal dispersion is, the higher is the activity. Therefore, herein, metal dispersion is clearly another parameter to determine the reforming activity, because the activities shown in Figure 1 and Figure 2 are almost proportional to the metal dispersion extent.

### HAADF–STEM mapping study on the reduced 7%Co–12%Ni/Al<sub>2</sub>O<sub>3</sub>

It is well-known that scanning transmission electron microscopy with energy-dispersive X-ray spectroscopy (STEM–EDX) mapping can provide clear image for element distributions. As an endeavor to further clarify the formation of Ni–Co alloys on

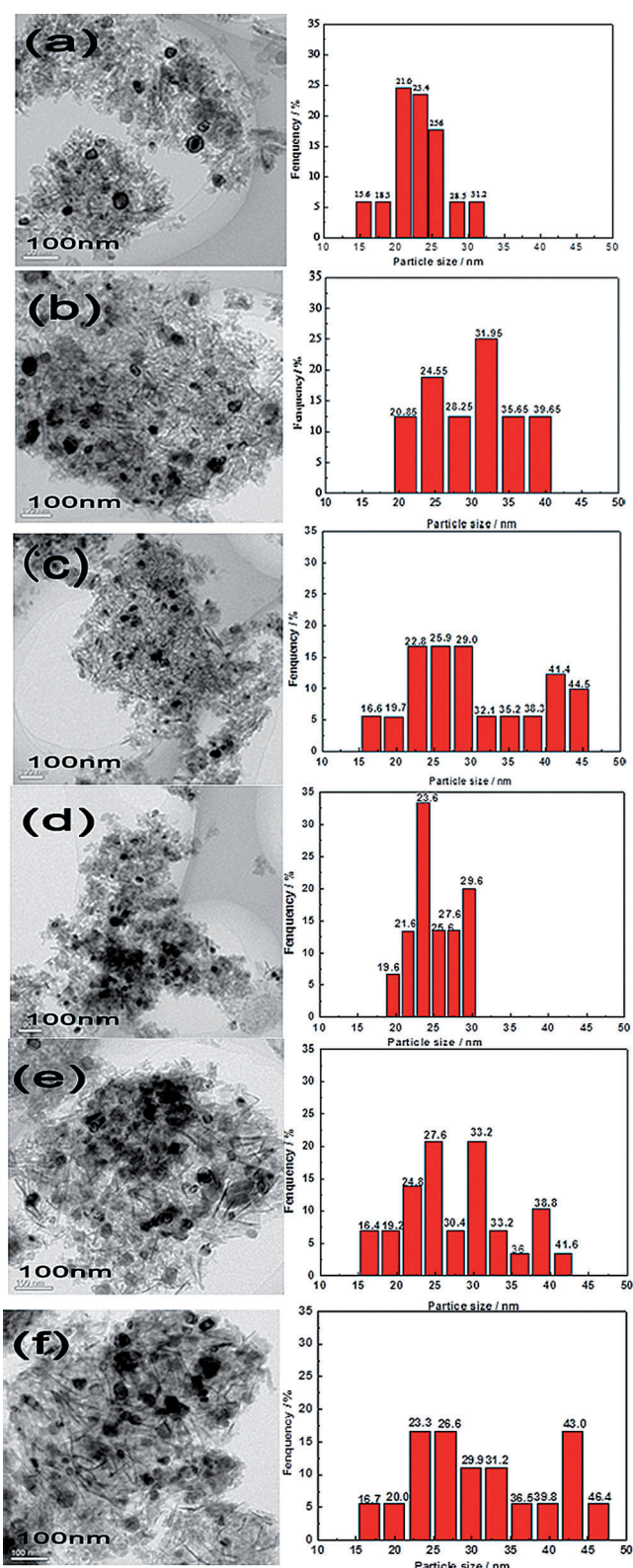


**Figure 9.** TEM images of the reduced catalysts with different Co contents. a) 12%Ni/Al<sub>2</sub>O<sub>3</sub>, b) 1%Co-12%Ni/Al<sub>2</sub>O<sub>3</sub>, c) 3%Co-12%Ni/Al<sub>2</sub>O<sub>3</sub>, d) 7%Co-12%Ni/Al<sub>2</sub>O<sub>3</sub>, e) 12%Co-12%Ni/Al<sub>2</sub>O<sub>3</sub>, f) 15%Co-12%Ni/Al<sub>2</sub>O<sub>3</sub>. Scale bars: a-f) 100 nm.

the surface of the reduced bimetallic catalysts, the fully reduced 7%Co-12%Ni/Al<sub>2</sub>O<sub>3</sub> catalyst, a typical sample in this

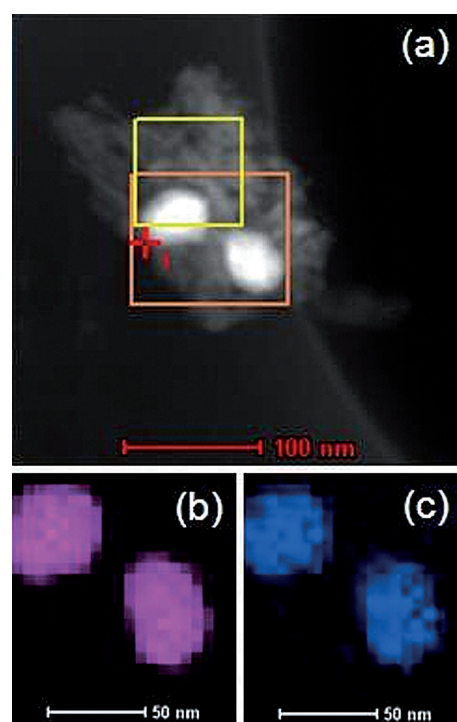


**Figure 10.** HAADF-STEM mapping of reduced 7%Co-12%Ni/Al<sub>2</sub>O<sub>3</sub> catalyst. a) Overview, b) Ni mapping image, c) Co mapping image. The boxes in (a) indicate the mapping zones. Scale bars: a) 100 nm, b) 50 nm, c) 50 nm

study, was thus subjected to HAADF-STEM mapping study. As shown in Figure 10 (a), the mapping zone is labelled by a “+” box. The two particles in the selected area have a mean size of approximately 30 nm, respectively. The Ni and Co mapping images are displayed in Figure 10 (b) and (c). The strong signals of both particles, which have the same shape, testify clearly that the two selected particles in the mapping zone consist of both Ni<sup>0</sup> and Co<sup>0</sup>, which provides direct and additional evidence to the XRD results that there is strong interaction between Ni<sup>0</sup> and Co<sup>0</sup> resulting in the formation of Ni-Co alloy on the surface of the reduced bimetallic catalysts.

## Discussion

Co-modified Ni-based catalysts have been extensively investigated for hydrogen production reactions, such as CH<sub>4</sub> dry reforming,<sup>[28,31,52]</sup> toluene and acetic acid steam reforming,<sup>[53]</sup> and tar cracking from biomass pyrolysis.<sup>[51]</sup> It has been commonly concluded that the Ni-Co bimetallic catalysts have significantly improved reaction performances compared to the corresponding monometallic Ni-based catalysts, especially for coke resistance, a critical issue for all the reforming reactions and catalysts. Studying CH<sub>4</sub> dry reforming, Zhang et al. ascribed the promotional effects to the improved Ni dispersion, the strong metal-support interaction, and the formation of solid solution by Co addition.<sup>[30,31]</sup> Yu et al. also found higher metal dispersion by Co addition.<sup>[36]</sup> In addition, Ni-Co alloy formation was also observed by them and several other groups,<sup>[27,30,32]</sup> which produces synergism effect between metallic Ni and Co, and

improves the coke resistance of the resulted catalysts. However, in the case of Ni-Co/TiO<sub>2</sub> catalysts for methane dry reforming, although Aika et al. also found the formation of Ni-Co alloy, they observed decreased Ni dispersion by Co addition,<sup>[37]</sup> which is in line with what found in this study. Despite the commonly accepted fact that Ni-Co bimetallic catalysts are good catalysts for various reforming reactions, there still exist some unclear issues for the promotional effects of Co on Ni-based catalysts, which deserve further study. In addition, to the best of our knowledge, Ni-Co bimetallic catalysts have rarely been introduced into MSR, especially supported on Al<sub>2</sub>O<sub>3</sub>, an important reaction currently employed for large-scale industrial hydrogen production. With the purpose to clarify the positive effects of Co on Ni, and eventually develop better catalysts with potent coke resistance and improved stability for natural-gas steam reforming, Ni-Co/Al<sub>2</sub>O<sub>3</sub> bimetallic catalysts were investigated for MSR in this study.

As a result, although the addition of Co decreased the reforming activity at low temperatures, the coke resistance as well as the reaction stability were improved significantly. Previously, it was found that the addition of Sn into Ni-based catalysts formed Ni-Sn alloys on the catalyst surface.<sup>[39,54,55]</sup> As a result, the activity of the Ni sites can be degraded, as evidenced by the improved activation energy of C-H bonds. The activity degradation was ascribed to the geometric and electronic changes of Ni sites induced by Sn, for example, Sn could block the low-coordinate Ni sites on Ni particles, which are actually the active sites for C-H activation, the rate-determining step for CH<sub>4</sub> reforming. Studying Au-modified Ni catalysts for steam reforming, Norskov et al. also found the formation of surface Au-Ni alloy, which improves the coke resistance of the bimetallic catalyst significantly but at the expense of the activity.<sup>[56]</sup> As with Sn-modified catalysts, the formation of Au-Ni alloy, as concluded by the authors, decreases the activity of the active sites. In the study herein, Ni-Co alloy formation was observed, as directly testified by XRD and TEM analyses and STEM-EDX mapping and indirectly evidenced by XPS and H<sub>2</sub>-TPR results. As a consequence, the active low-coordinate Ni sites could be blocked by alloy formation, as what occurred in the cases of Sn and Au modification. Therefore, compared with the activity of the unmodified Ni/Al<sub>2</sub>O<sub>3</sub> catalysts, the reforming activity at low temperatures was decreased by the addition of Co. In addition, Co addition also increased the crystallite and particle size of the metals, and decreased the metal dispersion and the specific surface areas of the bimetallic catalysts, which could also account for the lowered reforming activity. Therefore, the drop of the activity at low temperatures by Co modification, as shown in Figure 1, is reasonable.

As shown in Figure 3 and 4, with the addition of 7% Co, the severe coking of the original Ni/Al<sub>2</sub>O<sub>3</sub> can be completely suppressed. Therefore, no deactivation occurred to 7%Co-12%Ni/Al<sub>2</sub>O<sub>3</sub> during the 180 h test under the stringent condition (Figure 2). Although all the Co-modified catalysts have lower activity than the unmodified 12%Ni/Al<sub>2</sub>O<sub>3</sub> below 800 °C, at 800 °C, the general temperature for industrial operation for natural-gas steam reforming for syngas production, the initial methane conversion is the same for both the Co-modified and

unmodified catalysts. However, after 10 h reaction time, evident deactivation occurred to the unmodified 12%Ni/Al<sub>2</sub>O<sub>3</sub> catalyst, owing to severe coke formation. Based on the information provided in this study, further research on this catalyst system, such as tuning the Co/Ni ratios, optimizing the preparation condition and selecting better supports, could achieve active and stable catalysts for large-scale industrial application for natural-gas steam reforming.

## Conclusions

A series of supported bimetallic Ni-Co/ $\gamma$ -Al<sub>2</sub>O<sub>3</sub> catalysts with fixed 12% Ni loading but with different Co contents were prepared by the coimpregnation method and investigated for CH<sub>4</sub> steam reforming. The addition of Co can effectively improve the coke resistance of Ni/Al<sub>2</sub>O<sub>3</sub> and the reaction stability at a reasonable loss of the reforming activity at lower temperatures. At 800 °C, the regular operation temperature for industrial-scale natural-gas steam reforming, the Co-modified catalysts exhibit the same activity as the unmodified catalyst. XRD analyses and high-angle annular dark-field scanning transmission electron microscopy mapping of the reduced catalysts provided direct evidence for the observation that the addition of Co leads to the formation of surface Ni-Co alloys, which play a critical role in suppressing the coke formation of the bimetallic Ni-Co catalysts. However, the formation of Ni-Co alloy could also block part of the low-coordinated active Ni sites and decrease the metal dispersion, which is believed to be the major reason accounting for the lowered reforming activity of the Co-modified catalysts at lower temperatures. Based on the information from this work, improved natural-gas steam reforming catalysts with superior coke resistance and applicable activity could be designed and developed for large-scale industrial application.

## Experimental Section

### Catalyst preparation

The bimetallic Ni-Co catalysts supported on spherical  $\gamma$ -Al<sub>2</sub>O<sub>3</sub> (2–3 mm) were prepared by the impregnation method, with Ni(NO<sub>3</sub>)<sub>2</sub>·6H<sub>2</sub>O and Co(NO<sub>3</sub>)<sub>2</sub>·6H<sub>2</sub>O as the precursors.  $\gamma$ -Al<sub>2</sub>O<sub>3</sub> (800 °C 4 h calcined) support was added into the premixed aqueous solution of Ni(NO<sub>3</sub>)<sub>2</sub> and Co(NO<sub>3</sub>)<sub>2</sub> and stirred constantly for 24 h. Afterwards, the solution was heated at 80 °C until all the water was evaporated, then the mixture was further dried at 110 °C overnight and subsequently calcined in air atmosphere at 800 °C for 4 h. The catalysts were denoted by *m*%Co-12%Ni/Al<sub>2</sub>O<sub>3</sub>, because the Ni loading was always kept at 12 wt.%, but the Co loading varied from 1 wt.% to 15 wt.%. For comparison, 12%Ni/Al<sub>2</sub>O<sub>3</sub> and 12%Co/Al<sub>2</sub>O<sub>3</sub> were also prepared with impregnation method.

### Catalyst characterization

TGA-DSC was used to monitor the coke deposition amount of the spent catalysts. The experiments were performed with catalyst amounts of approximately 10 mg on a TA Q600 instrument with a ramping rate of 10 °Cmin<sup>-1</sup> from 25 to 800 °C in an air flow of 100 mLmin<sup>-1</sup>.

XRD method was used to analyze the phase composition of the freshly calcined and reduced catalysts. The experiments were performed on a Bruker AXS D8Focus diffractometer instrument operating at 40 kV and 40 mA with a Cu target and  $K\alpha$ -ray irradiation. Scans were collected over a range of  $2\theta$  degree from  $10^\circ$  to  $90^\circ$  with a step of  $0.03^\circ s^{-1}$ . The calculated experimental error for  $2\theta$  measurement of the peaks was  $\pm 0.01^\circ$ .

$H_2$ -TPR technique was used to study the effect of Co on the redox property of NiO species in the catalysts. The experiments were performed on a FINESORB 3010C instrument in a 10%  $H_2$ /Ar mixture gas flow, with the temperature increased from room temperature to  $900^\circ C$  at a rate of  $10^\circ C min^{-1}$ . Generally, a catalyst amount of 10 mg was used for the test. A thermal conductivity detector (TCD) was used to monitor the  $H_2$  consumption, and high-purity CuO (99.99%) was employed as a standard sample to quantify the  $H_2$  consumption.

$H_2$  adsorption-desorption was measured with a Micromeritics ASAP2020 system to analyze the Ni/Co metal dispersion on different supports. Typically, a catalyst amount of 50 mg was used for the test. The sample was reduced first in a  $30 mL min^{-1}$  10%  $H_2$ /Ar gas mixture flow at  $800^\circ C$  for 120 min and then purged by a  $30 mL min^{-1}$  ultra-high purity He flow at RT for 30 min before  $H_2$  adsorption in a  $20 mL min^{-1}$  10%  $H_2$ /Ar flow. Afterwards, the sample was purged again in a  $30 mL min^{-1}$  ultra-high purity He flow for 30 min to remove any physically adsorbed  $H_2$ . After getting a stable baseline, the temperature was increased to  $800^\circ C$  with a heating rate of  $10^\circ C min^{-1}$ . A  $H_2$  desorption peak was generally detected for each sample at approximately  $100^\circ C$ , and the relative  $H_2$  desorption amount of each sample was monitored with a TCD. For the quantification of the metal dispersion, a standard 0.5% Pt/ $Al_2O_3$  calibration sample provided by Micromeritics was used.

SEM images of the catalysts were taken on a Hitachi S-4800 field-emission scanning electron microscope. The TEM images were taken on a Tecnai F30 transmission electron microscope, and HAADF-STEM mapping analysis was performed on Oxford Instruments X-Max equipped with TEM F30.

XPS experiments were performed on a RBD upgraded PHI-5000C ESCA system by using a single  $MgK_{\alpha}$  X-ray source operating at 250 W and 14 kV. The spectra were obtained at ambient temperature with an ultrahigh vacuum. The binding energies were calibrated by using the C 1s peak of graphite at 284.6 eV as a reference.

### Catalyst activity evaluation

The catalysts were tested in a fixed-bed microreactor. Prior to reactions, generally a catalyst amount of 400 mg was reduced in situ in a 10%  $H_2$ /Ar flow at  $800^\circ C$  for 2 h. Afterwards, deionized water was pumped into a preheating chamber controlled at  $200^\circ C$  to evaporate it completely into steam, which was then mixed with  $CH_4$  (99.99%) flow at the stoichiometric  $H_2O/CH_4$  ratio of 2:1. The flow rate of pure  $CH_4$  was  $40 mL min^{-1}$ . The system pressure was 0.1 MPa, and the gas hourly space velocity (GHSV) was  $10800 mL g^{-1} h^{-1}$ . The outlet gas was cooled by ice water to trap the excess water vapor in the flow, and analyzed on-line on a GC9310 gas chromatograph equipped with a TDX-01 column and a TCD detector, using Ar as the carrier gas to monitor the amount of  $H_2$ , CO,  $CO_2$ , and  $CH_4$ .

### Acknowledgements

This work was supported by the Chinese Natural Science Foundation (21263015, 21203088), the Education Department of Jiangxi Province (KJLD14005, GJJ14205), and the Natural Science Foundation of Jiangxi Province (20142BAB213013), which is greatly acknowledged by the authors.

**Keywords:** alloys • cobalt • hydrogen • nickel • scanning probe microscopy

- [1] M. G. Schultz, *Science* **2003**, *302*, 624–627.
- [2] R. Kothari, D. Buddhi, R. L. Sawhney, *Renewable Sustainable Energy Rev.* **2008**, *12*, 553–563.
- [3] F. Qi, S. Howard, F. S. Maria, *Science* **2003**, *301*, 935–938.
- [4] S. Ayabe, H. Omoto, T. Utaka, R. Kikuchi, *Appl. Catal. A* **2003**, *241*, 261–269.
- [5] Y. Matsumura, T. Nakamori, *Appl. Catal. A* **2004**, *258*, 107–114.
- [6] R. R. N. Jens, S. Jens, K. N. Jens, *Adv. Catal.* **2002**, *47*, 65–139.
- [7] S. B. Wang, *Energy Fuels* **1996**, *10*, 896–904.
- [8] A. Arpornwichanop, M. Wasuleewan, *Int. J. Hydrogen Energy* **2011**, *25*, 929–934.
- [9] S. C. Baek, J. W. Bae, J. Y. Cheon, K. W. Jun, K. Y. Lee, *Catal. Lett.* **2011**, *141*, 224–234.
- [10] N. de Miguel, J. Manzanedo, P. L. Arias, *Chem. Eng. Technol.* **2012**, *35*, 2195–2203.
- [11] Y. S. Jung, W. L. Yoon, Y. W. Rhee, Y. S. Seo, *Int. J. Hydrogen Energy* **2012**, *37*, 9340–9350.
- [12] I. H. Son, S. J. Lee, A. Soon, H. S. Roh, H. Lee, *Appl. Catal. B* **2013**, *134–135*, 103–109.
- [13] Y. L. Zhao, Y. K. Lu, L. P. Chang, W. R. Bao, *J. Fuel Chem. Technol.* **2010**, *38*, 218–222.
- [14] X. Du, D. Zhang, L. Shi, R. Gao, J. Zhang, *J. Phys. Chem. C* **2012**, *116*, 10009–10016.
- [15] X. Du, D. Zhang, R. Gao, L. Huang, L. Shi, J. Zhang, *Chem. Commun.* **2013**, *49*, 6770–6772.
- [16] T. Xie, L. Shi, J. Zhang, D. Zhang, *Chem. Commun.* **2014**, *50*, 7250–7253.
- [17] D. L. Trimm, *Catal. Today* **1997**, *37*, 233–238.
- [18] C. J. Liu, J. Y. Ye, J. J. Jiang, Y. X. Pan, *ChemCatChem* **2011**, *3*, 529–541.
- [19] B. C. Zhang, X. L. Tang, Y. Li, Y. D. Xu, W. J. Shen, *Int. J. Hydrogen Energy* **2007**, *32*, 2367–2373.
- [20] Y. P. Li, T. J. Wang, C. Z. Wu, Y. Gao, X. H. Zhang, *Ind. Eng. Chem. Res.* **2010**, *49*, 3176–3183.
- [21] Z. Y. Hou, X. M. Zheng, T. Yashima, *React. Kinet. Catal. Lett.* **2005**, *84*, 229–235.
- [22] J. Li, D. Wang, G. D. Zhou, Y. X. Xue, C. Li, T. X. Cheng, *Ind. Eng. Chem. Res.* **2011**, *50*, 10955–10961.
- [23] Y. J. Bang, J. G. Seo, *Int. J. Hydrogen Energy* **2011**, *36*, 8307–8315.
- [24] H. Woo, R. Srinivasan, L. Rice, R. De Angelis, P. Reucroft, *J. Mol. Catal.* **1990**, *59*, 83–95.
- [25] I. Tatsumi, E. Koichi, A. Hiromichi, *Appl. Catal.* **1987**, *30*, 225–238.
- [26] P. C. Das, N. C. Pradhan, A. K. Dalai, N. N. Bakshi, *Catal. Lett.* **2004**, *98*, 153–160.
- [27] L. Chen, Q. S. Zhu, R. F. Wu, *Int. J. Hydrogen Energy* **2011**, *36*, 2128–2136.
- [28] D. S. José-Alonso, M. J. Illán-Gómez, M. C. Roman-Martínez, *Int. J. Hydrogen Energy* **2013**, *38*, 2230–2239.
- [29] P. Djinić, *Appl. Catal. B* **2012**, *125*, 259–270.
- [30] J. G. Zhang, H. Wang, A. K. Dalai, *Appl. Catal. A* **2008**, *339*, 121–129.
- [31] J. Zhang, H. Wang, A. K. Dalai, *J. Catal.* **2007**, *249*, 300–310.
- [32] A. C. W. Koh, L. W. Chen, W. K. Leong, B. F. G. Johnson, *Int. J. Hydrogen Energy* **2007**, *32*, 725–730.
- [33] I. Rossetti, J. Lasso, E. Finocchioni, G. Ramisb, V. Nichelec, *Appl. Catal. A* **2014**, *477*, 42–53.
- [34] X. Hu, G. X. Lu, *J. Mol. Catal. A* **2007**, *261*, 43–48.
- [35] L. W. Chen, C. K. S. Choong, Z. Y. Zhong, L. Huang, Z. Wang, J. Y. Lin, *Int. J. Hydrogen Energy* **2012**, *37*, 16321–16332.

- [36] Y. Yu, G. Q. Jin, Y. Y. Wang, X. Y. Guo, *Catal. Commun.* **2013**, *31*, 5–10.
- [37] K. Takanahe, K. Nagaoka, K. Nariai, K. C. Aika, *J. Catal.* **2005**, *232*, 268–275.
- [38] D. Harshini, Y. Kwon, J. Han, S. P. Yoon, S. W. Nam, T.-H. Lim, *Korean J. Chem. Eng.* **2010**, *27*, 480–486.
- [39] J. J. Liu, H. G. Peng, W. M. Liu, X. L. Xu, X. Wang, *ChemCatChem* **2014**, *6*, 2095–2104.
- [40] K. Tomishige, Y. Himeno, Y. Matsuo, Y. Yoshinaga, K. Fujimoto, *Ind. Eng. Chem. Res.* **2000**, *39*, 1891–1897.
- [41] X. Du, D. S. Zhang, L. Y. Shi, R. H. Gao, J. P. Zhang, *Nanoscale* **2013**, *5*, 2659–2663.
- [42] D. L. Trimm, *Catal. Rev.* **1977**, *16*, 155–189.
- [43] C. Wei, G. F. Zhao, Q. S. Xue, *Appl. Catal. B* **2013**, *136–137*, 260–268.
- [44] J. S. Choi, K. I. Moon, Y. G. Kim, J. S. Lee, C. H. Kimb, D. L. Trimm, *Catal. Lett.* **1998**, *52*, 43–47.
- [45] J. K. Xu, W. Zhou, Z. J. Li, J. H. Wang, J. X. Ma, *Int. J. Hydrogen Energy* **2009**, *34*, 6646–6654.
- [46] X. L. Xu, H. Han, J. J. Liu, W. M. Liu, W. L. Li, X. Wang, *J. Rare Earths* **2014**, *32*, 159–169.
- [47] Y. Lou, L. Wang, Z. Y. Zhao, Y. H. Zhang, Z. G. Zhang, G. Z. Lu, Y. Guo, Y. L. Guo, *Appl. Catal. B* **2014**, *146*, 43–49.
- [48] N. Muradov, F. Smith, A. T-Raissi, *Int. J. Hydrogen Energy* **2008**, *33*, 2023–2035.
- [49] S. Rana, S. Ram, *Mater. Sci. Technol.* **2005**, *21*, 243–249.
- [50] S. Y. Foo, C. C. Kui, T. H. Nguyen, A. A. Adesoji, *Int. J. Hydrogen Energy* **2012**, *37*, 17019–17026.
- [51] M. Lu, P. M. Lv, Z. H. Yuan, H. W. Li, *Renewable Energy* **2013**, *60*, 522–528.
- [52] Z. Hou, T. Yashimab, *Catal. Lett.* **2003**, *89*, 193–197.
- [53] S. Bona, P. Guillén, J. G. Alcalde, L. García, R. Bilbao, *Chem. Eng. J.* **2008**, *137*, 587–597.
- [54] E. Nikolla, A. Holewinski, J. Schwank, S. Linic, *J. Am. Chem. Soc.* **2006**, *128*, 11354–11355.
- [55] E. Nikolla, J. Schwank, S. Linic, *J. Am. Chem. Soc.* **2009**, *131*, 2747–2754.
- [56] F. Besenbacher, I. Chorkendorff, B. S. Clausen, B. Hammer, A. M. Molenbroek, J. K. Nørskov, *Science* **1998**, *279*, 1913–1915.

---

Received: August 31, 2014

Revised: September 18, 2014

Published online on October 30, 2014